The Astrophysical Journal Letters, 925:L6 (10pp), 2022 January 20 https://doi.org/10.3847/2041-8213/ac42d8

Solar Wind Ion Sputtering of Sodium from Silicates Using Molecular Dynamics Calculations of Surface Binding Energies

Liam S. Morrissey[1,2], Orenthal J. Tucker[2], Rosemary M. Killen[2], Sam Nakhla[3], and Daniel W. Savin[4]
[1] Catholic University/CRESST II, Washington, DC 20064, USA; lsm088@mun.ca
[2] NASA Goddard Space Flight Center, Greenbelt, MD 20771, USA
[3] Faculty of Engineering, Memorial University, St. John's, Newfoundland and Labrador, Canada
[4] Columbia Astrophysics Laboratory, Columbia University, New York, NY 10027, USA
Received 2021 October 1; revised 2021 December 9; accepted 2021 December 10; published 2022 January 24

Abstract

For nearly 40 yr, studies of exosphere formation on airless bodies have been hindered by uncertainties in our understanding of the underlying ion collisional sputtering by the solar wind (SW). These ion impacts on airless bodies play an important role in altering their surface properties and surrounding environment. Much of the collisional sputtering data needed for exosphere studies come from binary collision approximation (BCA) sputtering models. These depend on the surface binding energy (SBE) for the atoms sputtered from the impacted material. However, the SBE is not reliably known for many materials important for planetary science, such as plagioclase feldspars and sodium pyroxenes. BCA models typically approximate the SBE using the cohesive energy for a monoelemental solid. We use molecular dynamics (MD) to provide the first accurate SBE data we are aware of for Na sputtered from the above silicate minerals, which are expected to be important for exospheric formation at Mercury and the Moon. The MD SBE values are ∼8 times larger than the Na monoelemental cohesive energy. This has a significant effect on the predicted SW ion sputtering yield and energy distribution of Na and the formation of the corresponding Na exosphere. We also find that the SBE is correlated with the coordination number of the Na atoms within the substrate and with the cohesive energy of the Na-bearing silicate. Our MD SBE results will enable more accurate BCA predictions for the SW ion sputtering contribution to the Na exosphere of Mercury and the Moon.

Unified Astronomy Thesaurus concepts: Slow solar wind (1873); Surface processes (2116); Mercury (planet) (1024); Lunar surface (974); Exosphere (499)

1. Introduction

For nearly 40 yr, planetary science studies into the formation of the exospheres of Mercury, the Moon, and other airless bodies have been hindered because of uncertainties in our understanding of the underlying ion sputtering process by the solar wind (SW) that is predicted to contribute to the exospheric formation. One major hindrance is due to the well-known uncertainties in the surface binding energies (SBEs) of the observed exospheric atoms in their expected mineral sources on the planetary surfaces (McGrath et al. 1986; Elphic et al. 1991; Killen et al. 2001; Lammer et al. 2003; Pieters et al. 2009; Wurz et al. 2010; Schaible et al. 2017; Szabo et al. 2020).

Molecular dynamics (MD) calculations are an accurate means to generate accurate SBEs, as has been demonstrated in comparisons to benchmark laboratory measurements (Morrissey et al. 2021). Some early MD calculations for SBEs of monoelemental metals were performed by Jackson (1973, 1975) and Gades & Urbassek (1994). More recently, MD calculations have been published for the Si-bearing compound SiC (Bringuier et al. 2019). However, we are unaware of any such MD calculations for silicate mineral compounds that play an important role in planetary science. Theoretical work by Gades & Urbassek (1994) presents a scaling relationship to determine the SBEs for alloys using monoelemental cohesive energies. However, as we will show below, these scaling methods cannot be reliably applied to determine SBEs for the silicate minerals that are abundant on the surfaces of rocky planets.

Of particular interest is sodium (Na), which has been detected in the surface-bounded exospheres of the Moon and Mercury. Though only a trace element on the their surfaces, Na is easily detectable in their exospheres (McGrath et al. 1986; Potter & Morgan 1988; Killen & Ip 1999; Mura et al. 2009; Schmidt et al. 2012, 2020; Peplowski et al. 2014; Colaprete et al. 2016; Song et al. 2016; Killen et al. 2019, 2021). The source of this exospheric Na may be due to processes such as photon-stimulated desorption (PSD), impact vaporization (IV), and SW ion irradiation. This exospheric Na has been observed on the dayside at higher altitudes than expected (Leblanc et al. 2008; Vervack et al. 2010; Mouawad et al. 2011; Killen et al. 2021), suggesting the need for an energetic emission process. PSD ejects Na atoms with energies too low to explain the high-altitude dayside abundances (Burger et al. 2010; Schmidt et al. 2012; Tenishev et al. 2013; Gamborino et al. 2019). IV also does not eject atoms with sufficiently high energies (Schmidt et al. 2012).

SW ion sputtering is the most likely candidate to explain the dayside high-altitude Na abundances. When SW ions hit a surface, they can sputter atoms from the impacted material (Killen et al. 2001; Domingue et al. 2014). SW ions can induce two types of sputtering: electronic and collisional. Electronic sputtering results when the ions excite bound electrons in the substrate, forming repulsive electronic states of the atoms in the substrate (Johnson 2013).[5] However, electronic sputtering

[5] "Electronic sputtering" can also refer to energy transfer between an incident ion and substrate electrons that then couple to phonons. This causes a localized thermal spike, leading to the removal of atoms by evaporation from the locally heated volume. This processes is dominant at MeV amu^{-1} impact energies but insignificant at SW energies of 1 keV amu^{-1} (Assmann et al. 2007; Behrisch & Eckstein 2007).

produces ejecta at low energies (Madey et al. 1998) and cannot explain the dayside high-altitude Na exosphere on the Moon or Mercury. Collisional sputtering refers to the emission of target atoms from collisions between nuclei, either the incident ion and an atom in the substrate or from the resulting collision cascade within the substrate (Behrisch & Eckstein 2007). Collisional sputtering typically dominates at energies below 100 keV amu^{-1} (Krasheninnikov & Nordlund 2010) and is the only process that can potentially eject particles with sufficient energies to explain the observed dayside high-altitude Na exosphere on the Moon (Killen et al. 2021) and Mercury (Mouawad et al. 2011). Here we study collisional sputtering of Na by SW ions.

The lunar surface is continually bombarded by SW ions because the Moon does not possess an atmosphere or intrinsic magnetic field to shield the surface (Poppe et al. 2018; Tucker et al. 2021). On Mercury, SW ions impact the surface through the high-latitude dayside cusps associated with the magnetic poles (Raines et al. 2013) and the mid-latitude nightside through magnetotail reconnection (Fatemi et al. 2020). On both bodies, surficial Na is inferred to be contained in plagioclase feldspars and to a lesser extent in sodium pyroxenes, both silicate minerals (Papike et al. 1991; McClintock et al. 2018; McCoy et al. 2018). Hence, understanding SW-induced sputtering of Na from silicates is needed to interpret ground-based and spacecraft observations of exospheric Na for the Moon and Mercury (Leblanc & Johnson 2003; Killen et al. 2007; Sarantos et al. 2007; Mura et al. 2009; Wurz et al. 2010; Cassidy et al. 2016; Kallio et al. 2019).

The most common collisional sputtering models use the binary collision approximation (BCA), which treats sputtering as the result of binary collision cascades involving atomic nuclei (Eckstein & Urbassek 2007). Commonly used BCA models include the Thompson model (Thompson 1968) and the Monte Carlo code Transport Range of Ions in Matter (TRIM; Ziegler & Biersack 1985). Another model is SDTrimSP (Mutzke et al. 2019), an extension of TRIM that can be run in standard (S) or dynamical (D) mode (which tracks compositional changes in the impacted substrate) using either serial (S) or parallel (P) processing. The Thompson model predicts the ejecta energy distribution versus the incident ion energy. TRIM and SDTrimSP predict the ejecta energy distribution and yield as a function of incoming ion type, energy, and angle, with only modest computational requirements. The Thompson model does not account for electronic losses. TRIM and SDTrimSP both account for collisional (i.e., nuclear) and electronic losses during the collision process. For our ejecta energy distribution results here, we have used the Thompson model. For our sputtering yield results, we have used SDTrimSP.

A fundamental parameter for all BCA models is the SBE of the atoms in the impacted substrate (Kelly 1986; Behrisch & Eckstein 2007). The sputtered atom energy distribution given by Thompson theory (Thompson 1968) is given by the analytic expression

$$J(E) \propto \frac{E}{(E + E_b)^3}. \quad (1)$$

Here E is the sputtered ion energy and E_b is the SBE of the sputtered atom. This distribution peaks at $E_b/2$ and at higher emission energies ($E \gg E_b$) follows an E^{-2} power law. SBE is also used for empirically derived formulae (Yamamura & Tawara 1996; Eckstein 2007) that predict the sputtering yield as a function of the incoming atom and target type.

Despite the importance of the SBE for sputtering models, its value is not well defined for many substrates. For monoelemental substrates, the SBE is often approximated as the monoelemental sublimation energy, equal to the cohesive energy E_{coh} for the ground state of the individual atoms in the substrate (Gschneidner 1964; Behrisch & Eckstein 2007):

$$E_{coh} = \frac{E_T}{N}. \quad (2)$$

Here E_T is the total potential energy of the system and N is the number of atoms in the system. This is the method used both for our MD results presented here and by the density functional theory (DFT) results of Jain et al. (2013). For compounds E_{coh} is calculated as a single value using the total potential energy for all element types. Theoretical studies of monoelemental solids find that the SBE is 30%–40% larger than E_{coh} (Yang & Hassanein 2014; Morrissey et al. 2021). The monoelemental E_{coh} of a given element is also often used for its SBE in a multicomponent substrate (Mutzke et al. 2019), a questionable assumption discussed below. For alloys, Gades & Urbassek (1994) concluded that SBEs scale linearly with concentration and depend mainly on monoelemental cohesive energies within the alloy. However, alloys are distinctly different from minerals, and changes in concentration within an alloy are not analogous to different elemental concentrations for different minerals. We discuss this further in Section 3. Other multicomponent substrate studies have treated the SBE as a fitting parameter to experimental energy distributions and yields (Behrisch & Eckstein 2007).

Planetary surfaces are not elementally pure. SBE values are needed for multicomponent compounds, but accurate values are lacking. For Na, a large range of values have been used for SW sputtering models. Based on the laboratory studies of Wiens et al. (1997) for Na ejected from sodium sulfate (Na_2SO_4), Leblanc & Johnson (2003) recommended an SBE of 0.27 eV. SDTrimSP recommends using the monoelemental E_{coh} for each element in a multicomponent compound, with 1.1 eV prescribed for Na (Mutzke et al. 2019). However, this approach makes the questionable assumption that the SBE of an atom is independent of the bonds formed with other atom types in the compound. In a study of Na release rates on Mercury, Lammer et al. (2003) used SBE values between 2 and 2.65 eV but noted that these choices require experimental verification. Subsequently, Mura et al. (2007) have investigated the effects of an Na SBE between 1 and 4 eV but favor values at the lower end of this range based on the work of Leblanc & Johnson (2003). Most recently, Werner et al. (2022) used an SBE of 0.27 eV to model the SW sputtering contribution to Mercury's Na exosphere.

Uncertainties in the SBE can be a significant source of error for BCA sputtering predictions from multicomponent substrates and hinder our understanding of the formation of the exospheres of the Moon and Mercury. This has resulted in numerous calls for more accurate multicomponent SBEs from compounds and minerals (McGrath et al. 1986; Lammer et al. 2003; Behrisch & Eckstein 2007; Mura et al. 2007; Szabo et al. 2020). Recent research has suggested that MD simulations offer a viable and accurate method for determining SBEs (Urbassek 2007; Bringuier et al. 2019; Morrissey et al. 2021).

MD simulations use an interatomic potential to model all atomic interactions in the system. However, this requires a significant computational effort, limiting the size, duration, and impact energies that can be reasonably simulated. It is computationally more tractable to use MD to obtain elemental SBE values for specific compounds. These results can then be input into computationally more efficient BCA methods to predict the yield and energy distributions of sputtered atoms due to SW impacts. Previous work has shown that BCA and MD results are in good agreement for predicted sputtering yields and ejecta energy distributions (Yang & Hassanein 2014; Morrissey et al. 2021). In our work, we use MD to provide the first accurate SBE data that we are aware of for Na being sputtered for a range of silicates that are expected to be important for exospheric formation at Mercury and the Moon.

One open question beyond the scope of this work is the fraction of Na sputtered as an atom versus as an ion. There have been several experimental studies of Na^+ emission from sputtering, but these have been unable to quantitatively determine the relative sputtered Na and Na^+ abundances (Elphic et al. 1991; Dukes et al. 2011; Martinez et al. 2017). Most relevant is Dukes et al. (2011), where they investigated 4 keV He^+ sputtering from albite and suggest that the Na is primarily sputtered as an Na^+, but these findings are counter to sputtering studies of other elements that have measured ion-to-neutral ratios (Mazarov et al. 2006; Behrisch & Eckstein 2007). Considering that Na at high altitudes in the Hermean exosphere has been primarily detected through resonant scattering of solar radiation by neutral Na (Leblanc et al. 2008; Vervack et al. 2010), we focus on sputtered Na neutrals from silicates. However, whether Na is sputtered as a neutral or ion is likely to have little impact on the ejecta energy distribution. Previous measurements on sputtered Ba from barium oxide, copper, and indium have found that sputtered neutrals and ions have similar energy distributions (Lundquist 1978; Grischkowsky et al. 1983; Betz 1987; Mazarov et al. 2006). The BCA method we use here tracks how collision cascades develop within the target but does not account for the charge states of the incident ion, the substrate, or the sputtered particles.

The remainder of this paper is as follows: Section 2 presents the MD approach used to calculate E_{coh} and the Na SBE from various silicates. Also described are the BCA models to determine the ejecta energy distribution and sputtering yield. Section 3 presents the compound-specific E_{coh} and Na SBE values from MD simulations, compares them to published values, and explores the effect of these SBE values on the BCA-predicted sputtering yield and ejecta energy distribution. The planetary science implications are then briefly discussed. Section 4 concludes with a discussion on the role MD simulations can play in obtaining compound-specific SBEs for planetary science.

2. Methodology

2.1. Molecular Dynamics Simulations: Surface Binding and Cohesive Energies

We have used MD simulations to calculate the Na SBE from both pure Na and Na-bearing compounds. The pure Na SBE was used to test the assumption that the SBE for a monoelemental solid can be estimated as E_{coh}. Various Na-bearing silicates were then considered. Sodium metasilicate (Na_2SiO_3) and sodium orthosilicate (Na_4SiO_4) were chosen for their simplicity. Lunar sample returns have shown that Na is largely found in plagioclase feldspar and to a lesser extent in sodium pyroxenes and that both are of intermediate composition (Papike et al. 1991). Mercury observations suggest that the surface Na is contained in intermediate-composition plagioclase feldspars (Papike et al. 1991; Sprague et al. 2002; Domingue et al. 2014; Peplowski et al. 2014; McClintock et al. 2018; McCoy et al. 2018). For computational simplicity, we performed MD calculations using the plagioclase feldspar endmember albite ($NaAlSi_3O_8$) and the sodium pyroxene endmember jadeite ($NaAlSi_2O_6$). In addition, for comparison to available experimental data, we also performed MD simulations on nepheline ($NaAlSiO_4$), an Na-bearing tectosilicate that has been considered as a simulant for several solar system planetary bodies (Martinez et al. 2017).

MD calculations were performed using the Large-scale Atomic/Molecular Massively Parallel Simulation (LAMMPS) package (Plimpton 1995). Interactions between atoms in each compound considered were simulated using a reactive force field (ReaxFF) empirical potential that allows for the dynamic simulation of bond breaking and reformation in a multi-component substrate (Van Duin et al. 2001). ReaxFF is uniquely able to simulate both bonded and nonbonded interactions. Connectivity-dependent reactions (valence and torsion energy) are modeled so that when bonds are broken their contribution to the total energy is zero. Nonbonded interactions, van der Waals and long-range Coulomb, are calculated irrespective of the connections between all atom pairs in the simulation. Therefore, ReaxFF potentials do not require the use of long-range interaction methods such as Ewald (Darden et al. 1993) and Wolf (Wolf et al. 1999). Coulomb interactions are cut off at a standard distance of 10 Å. More details are given in Van Duin et al. (2001). For our study, we selected a ReaxFF potential developed by Pitman & Van Duin (2012) and modified by Lyngdoh et al. (2019) for structures composed of Na, Al, Si, and O. This potential has been validated for a range of crystalline sodium silicate structures, including albite, and has demonstrated accurate descriptions of both bulk and surface properties (for additional details see Lyngdoh et al. 2019). In addition to this potential, we also used a ReaxFF potential parameterized for silicate structures composed of Na, Si, and O by Hahn et al. (2018). This potential was parameterized using volume–energy relations of Na silicates, Na migration energy, and Na interactions with surfaces. In addition, the potential was specifically optimized and verified for Na–O bond energies along with the equations of states for several Na silicates (for additional details see Hahn et al. 2018).

For our SBE calculations for both the Lyngdoh et al. (2019) and Hahn et al. (2018) potentials, we developed crystalline targets with ~5000 atoms and dimensions of approximately $40 \times 40 \times 50$ Å in the x, y, and z directions, respectively. The simulation domain extended 100 Å above the free surface. Boundary conditions were periodic in x and y and fixed in z to simulate an infinite slab with constant thickness and a free surface. The system then underwent a charge equilibration using the Electron Equilibration Method approach (Mortier et al. 1986) as implemented in LAMMPS (Plimpton 1995) and described by Van Duin et al. (2001) to minimize the electrostatic energy by adjusting partial charges on individual atoms based on neighbor interactions. Next, a Berendsen barostat followed by a Berensden thermostat (Berendsen et al. 1984) were used to relax the target and equilibrate it to 1 K and 0 atm. The bottom three layers of the target were fixed in space (Figure 1(a)). Similar to the method of Yang & Hassanein (2014), for each substrate a random surface

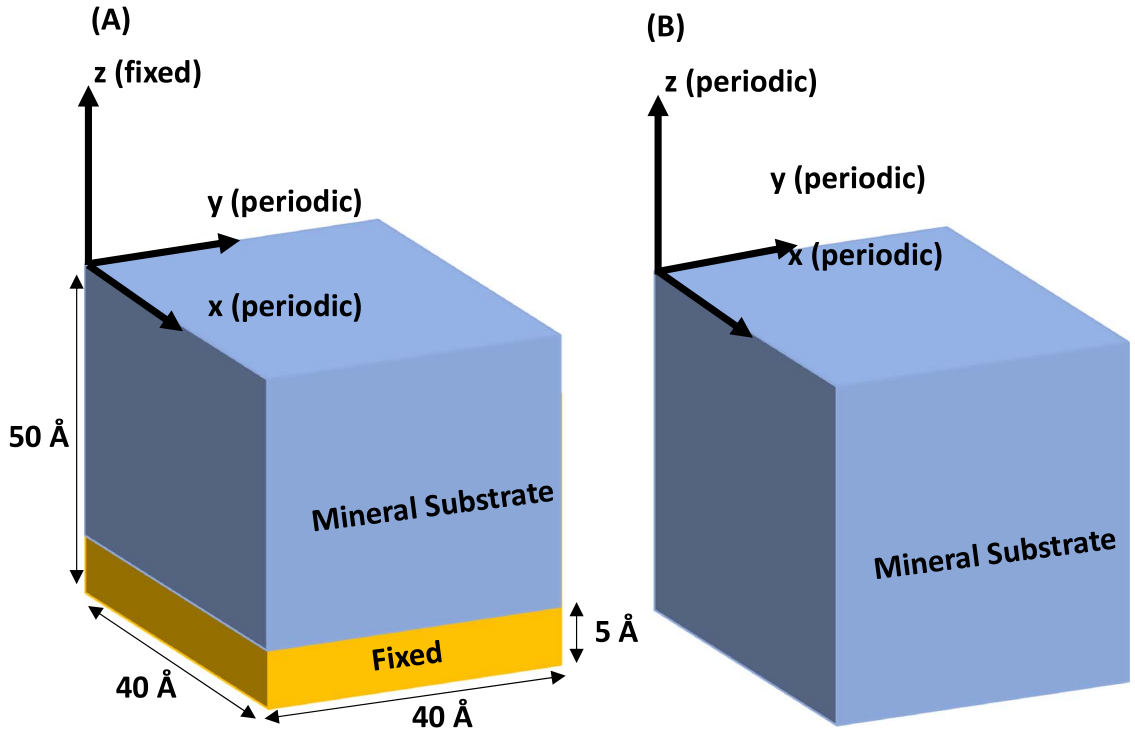

Figure 1. Schematic of the MD substrate used to calculate the (a) Na SBE and (b) E_{coh} from the simulated targets. The substrate is shown in blue, and the three fixed layers are shown in yellow.

Na atom was then given a specific kinetic energy and its subsequent position and remaining energy were tracked versus time. An iterative method was used to determine the minimum energy needed to remove one Na atom completely from the surface. The Na atom was considered emitted when it has separated far enough that it no longer interacts with the surface, i.e., it experiences no attractive or repulsive forces and the energy remained constant. For each case, five random Na surface atoms were tested to verify the repeatability of the results. No differences in the resulting SBEs for a given substrate were expected or found, as for each substrate considered the Na in the crystal unit cell occupied only one surface position; hence, we do not quote error bars.

We also calculated E_{coh} for each target using MD. For this we developed a crystalline bulk slab with periodic boundary conditions in the x, y, and z directions to avoid surface effects (Figure 1(b)). This slab was then relaxed using the same equilibration procedure as before. After this, a minimization was performed to allow all atoms to reach their local potential energy minimum.

2.2. BCA Model Simulations

BCA models were used to investigate the effects of compound-specific SBEs on the predicted Na sputtering yield and energy distributions. The BCA method tracks the kinetic energy of atoms within the impacted substrate but does not account for atomic ionization or ionic neutralization that might occur in the substrate or as the particle leaves the substrate. We used the analytic Thompson relationship, Equation (1), to study how the predicted energy distributions of the sputtered Na varied with SBE. We used SDTrimSP to investigate the sputtered atom yield versus SBE. The Thompson relationship considers only the kinetic energy of the incident ion, but not the type, and the sputtered atom type, while SDTrimSP allows users to define the kinetic energy and a specific ion/target combination.

To capture the most common SW component, we simulated 1 keV H^+ impacts. For the target, we selected albite. A range of Na SBEs were tested, using previously reported values and our MD values. As recommended by the SDTrimSP manual, SBEs for all other elements in the compound were left at their monoelemental E_{coh}. Following Möller & Posselt (2001) and Szabo et al. (2020), the elemental density of oxygen in the albite was modified in SDTrimSP to achieve a bulk density of 2.62 g cm^{-3}, matching experimental data (Mineral Data Publishing 2001). Only impacts normal to the surface (a polar angle of 0°) were considered. We expect that the yield would increase with larger incident polar angles (Behrisch & Eckstein 2007). A total of 10^6 impacts were statically simulated for each SBE on a 5000 Å thick albite slab. SDTrimSP simulations were carried out allowing the SBE of each atom type to be defined separately.

3. Results and Discussion

3.1. Simulated Surface Binding and Cohesive Energies

The MD calculations using the Lyngdoh et al. (2019) potentials are given in Table 1. These data include the corresponding coordination number, cohesive energies, and SBEs from our MD simulations. Also given are the cohesive energies from DFT calculations as provided by the Materials Project database (Jain et al. 2013) using the Vienna Ab Initia Simulation Package. DFT is an ab initio quantum mechanical method to simulate the electronic structure of many-body systems. We note that DFT cannot calculate SBEs. We found a large range in the simulated MD E_{coh}, from 0.9 eV atom^{-1} for pure Na to 6.4 eV atom^{-1} for albite. For pure Na, the MD E_{coh} was 0.2 eV lower than the DFT and experimental values. On

Table 1
E_{coh} and Na SBE for a Range of Na-bearing Substrates

Target	Formula	Na Concentration c_{Na}	E_{coh} (eV atom^{-1})				Na SBE (eV)		Na Coordination Number, Z
			MD[a]	MD[b]	DFT	Experiment	MD	Experiment	
Pure sodium	Na	100%	0.9	0.8	1.1	1.1[c]	1.4	⋯	⋯
Sodium orthosilicate	Na_4SiO_4	44%	4.4	4.5	4.9	⋯	2.6	⋯	4
Sodium metasilicate	Na_2SiO_3	33%	5.2	5.1	5.5	⋯	4.4	⋯	5
Nepheline	$NaAlSiO_4$	14%	5.8	⋯	5.6	⋯	4.8	≈4.8[d]	6
Albite	$NaAlSi_3O_8$	8%	6.4	⋯	6.7	⋯	7.9	⋯	7
Jadeite	$NaAlSi_2O_6$	10%	6.3	⋯	6.6	⋯	8.4	⋯	7

Notes.
[a] MD potential by Lyngdoh et al. (2019).
[b] MD potential by Hahn et al. (2018).
[c] Kittel et al. (1996).
[d] Martinez et al. (2017).

average, E_{coh} from MD was slightly lower than DFT. To confirm that this was not an issue with the potential, identical simulations were run on sodium metasilicate and sodium orthosilicate, using the ReaxFF potential for Na–Si–O systems of Hahn et al. (2018), with the resulting SBEs given in Table 1. We obtained cohesive energies that were within 4% of the Lyngdoh et al. (2019) ReaxFF potential and that were also below the DFT values. For pure Na, using the Hahn et al. (2018) potentials, the predicted E_{coh} was 0.8 eV atom^{-1}, 0.3 eV lower than the DFT and experimental values. The range of agreement between the two different ReaxFF results and the DFT results provides an estimate for the uncertainty in our theoretical SBE results of about 0.2 eV.

We found a large range in MD Na SBE values (Table 1), depending on the substrate considered. For all substrates considered, the partial charge of the separated Na as calculated by ReaxFF was approximately 0.3. The SBE is lowest for pure Na, at 1.4 eV. This is 40% higher than the MD monoelemental E_{coh}, a difference that is similar to previous MD simulations by Yang & Hassanein (2014) for pure tungsten and beryllium. The SBE increases going from pure Na to the silicates considered and is highest for albite (7.9 eV) and jadeite (8.4 eV). Additionally, while all the minerals considered contain Na–O bonds, they all have different Na SBE values. These findings highlight the importance the actual mineral structure has on the SBE. Furthermore, as E_{coh} of the mineral increases, and as more bonds are formed with each Na atom, the SBE increases. The detailed physics or chemistry for the origin of this variety is empirically included in the MD calculations. Identifying the specific mineral properties that cause this variability is beyond the scope of this work. But our logical inference provides a direction for future research on this subject.

Our MD results also demonstrate the shortcomings of the approach most commonly used to estimate SBEs from multielemental materials, which is to approximate the SBE for each element by its monoelemental E_{coh} (e.g., in TRIM or SDTrimSP). For alloys, Gades & Urbassek (1994) proposed that the SBE scaled linearly with elemental concentration and was a function of the monoelemental cohesive energy of each element. However, we find that this linear relationship does not hold for Na-bearing minerals (see Appendix). Bringuier et al. (2019) used MD to demonstrate that the SBE of Si and C in SiC, a semiconductor, was discrepant from their monoelemental cohesive energies. However, their work was limited to SiC only and did not consider the effect on sputtering behavior or compare these findings to experimental measurements.

Table 2
Na Sputtering Yield Using SDTrimSP for Various Na SBE Values for 1 keV H^+ Impacting an Albite Surface at Normal Incidence

Na SBE (eV)	Na SBE Source	Sputtering Yield
0.27	Sodium sulfate[a]	1.15E-02
1.1	DFT E_{coh}[b]	6.04E-03
1.4	Pure sodium[c]	4.61E-03
2.6	Sodium orthosilicate[c]	2.09E-03
4.4	Sodium metasilicate[c]	1.00E-03
4.8	Nepheline[c]	8.28E-04
7.9	Albite[c]	4.12E-04
8.4	Jadeite[c]	3.71E-04

Notes.
[a] Wiens et al. (1997).
[b] Mutzke et al. (2019).
[c] Present MD results using Lyngdoh et al. (2019) potential.

3.2. Effect of Surface Binding Energy on Sputtering Behavior

The SDTrimSP-simulated sputtering yield of Na from albite versus SBE is shown in Figure 2 using the Na SBEs given in Table 2, which also lists the associated Na sputtering yield. As expected, with increasing SBE there is a decrease in the predicted sputtering yield. Increasing the SBE from 0.27 to 7.9 eV decreases the Na sputtering yield by a factor of 28. Furthermore, the predicted yield using the 1.1 eV E_{coh} of Na was approximately 3–15 times higher than the yield using SBEs for Na from sodium silicates. Clearly, the yield by approximating the SBE as the monoelemental E_{coh} is highly discrepant relative to that using compound-specific SBEs.

The effect of the Na SBE on the predicted ejecta energy distribution is given in Figure 3, using the analytic Thompson distribution. In our previous work (Morrissey et al. 2021), we showed that there is excellent agreement between the Thompson distribution and SDTrimSP results for ejecta energy distributions due to 1 keV impactors. Figure 3 shows that the peak in the distribution occurs at $E_b/2$, as expected. For larger SBEs, the peak shifts to higher energies and the width of the distribution increases. Increasing the SBE from 0.27 to 7.9 eV linearly increases the peak of the energy distribution by a factor of ∼30 and the FWHM by a factor of ∼28. For the four silicates tested in

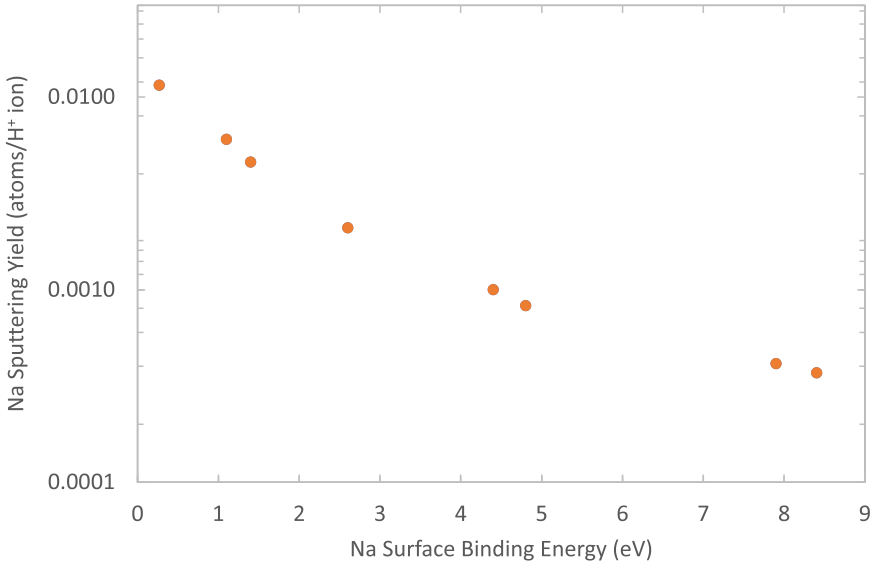

Figure 2. Na sputtering yield vs. Na SBE using SDTrimSP for 1 keV H^+ impacting an albite surface at normal incidence.

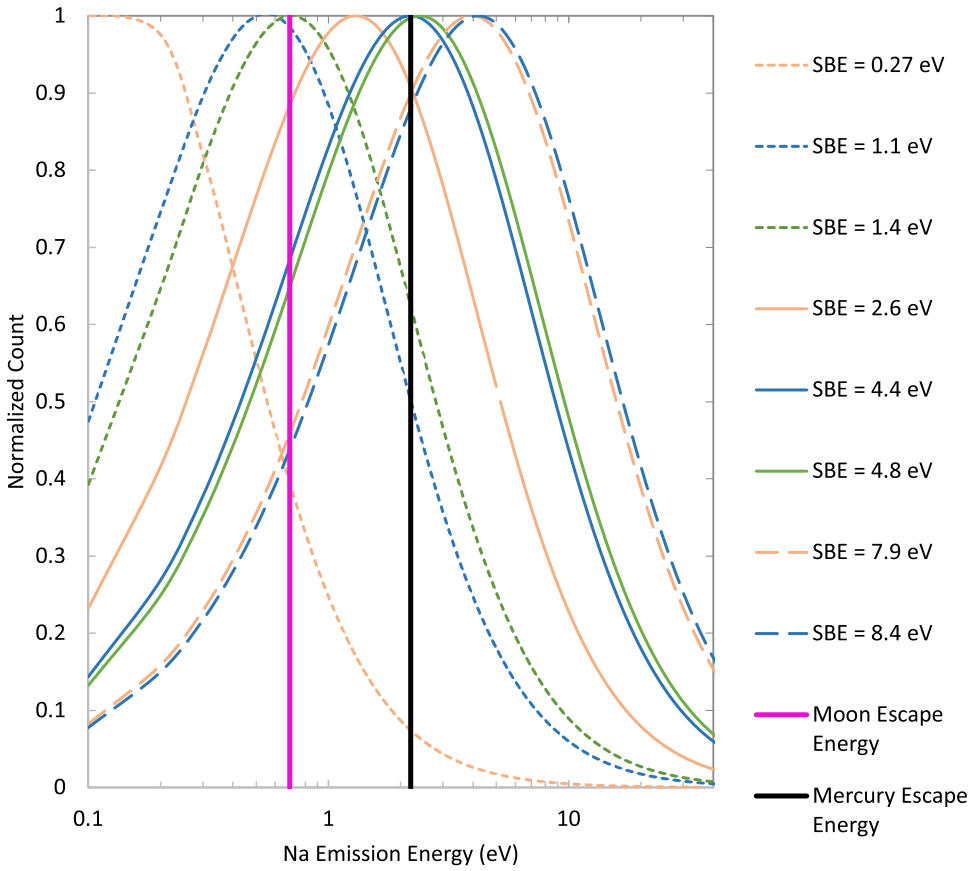

Figure 3. Energy distribution of sputtered Na atoms vs. SBE using the analytic Thompson distribution. The escape energies for an Na atom from the Moon (0.7 eV) and Mercury (2.2 eV) are shown by the magenta and black solid lines, respectively.

MD, increasing the SBE from 2.6 to 8.4 eV increases the peak energy distribution and the FWHM by factors of ∼3.

There are few experimental measurements of the yields and energy distribution for Na sputtered from silicates. Martinez et al. (2017) measured the energy distribution of sputtered Na^+ from nepheline and observed a peak in the distribution at ≈2.4 eV, corresponding to an SBE of ≈4.8 eV. Our simulated results for nepheline, which did not account for ionization state, predict an Na SBE in excellent agreement with that inferred from the Na^+ measurements of Martinez et al. This supports previous experimental conclusions that sputtered neutrals and ions have similar energy distributions (Lundquist 1978; Grischkowsky et al. 1983; Betz 1987; Mazarov et al. 2006). Furthermore, the agreement between the MD and experimental SBE in nepheline

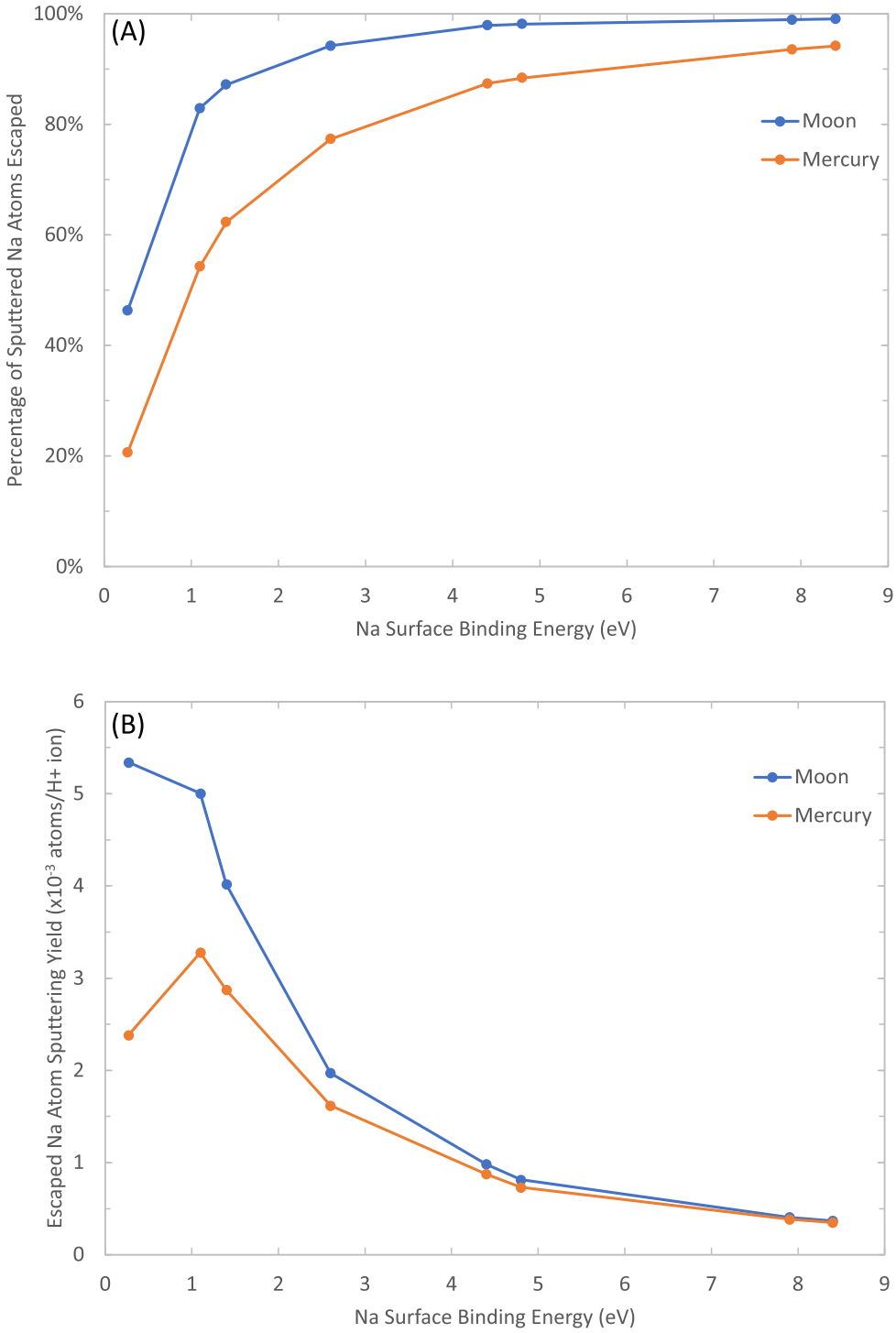

Figure 4. (a) Percentage of sputtered Na atoms with an energy above the escape velocity of the Moon (blue points) and Mercury (orange points). (b) The corresponding sputtering yield of escaped Na atoms per H atom. In both panels (a) and (b) the lines are drawn to guide the eye.

supports the conclusion that SBE is a compound-specific value that can be accurately calculated using MD simulations. It also demonstrates that SBE is not a fitting parameter but an intrinsic quantity describing the physical properties of the substrate.

Dukes & Baragiola (2015) also measured the energy distribution of sputtered Na^+ ions from two different lunar soil samples. In those samples, the Na is again likely contained within a silicate. However, the lack of mineral purity in each sample hinders a reliable interpretation of the sputtered Na^+ energy distribution.

Lastly, we note that Leblanc & Johnson (2003) derived an Na SBE of 0.27 eV from the Wiens et al. (1997) measurements that used laser post-ionization data of Na neutrals sputtered from sulfates. Wiens et al. (1997) also measured high-energy secondary Na^+ yields but determined that those measurements were likely affected by the experimental setup. Sodium sulfate

has an E_{coh} of 5.1 eV and an Na coordination number of 6 (Jain et al. 2013). Based on the MD values for sodium silicates, this would suggest an Na SBE much larger than the inferred 0.27 eV. The cause of this potential discrepancy is beyond the scope of this study. However, we will investigate the issue in a future study.

3.3. Implications for Sputtering Contribution to Exospheres

Ejecta energy distributions are important in exosphere models for determining the number of atoms with sufficient energy to escape the celestial body (Killen et al. 2004). As the SBE increases, there is a significant increase in the percentage of sputtered Na atoms with energies exceeding the escape velocity of the Moon, 2.4 km s^{-1} corresponding to 0.7 eV, and Mercury, 4.3 km s^{-1} corresponding to 2.2 eV (Figure 4(a)). For an SBE input of 0.27 eV, only 43% and 21% of sputtered Na atoms exceed the escape velocity for the Moon and Mercury, respectively. As the Na SBE increases to that of sodium silicates, the percentage of sputtered atoms exceeding the escape energy increases. For the Na SBE from albite, over 90% of sputtered atoms are ejected with an energy above the escape energy of the Moon and Mercury. However, this percentage needs to be multiplied by the sputtering yield to obtain the Na sputtering yield above the escape energy (Figure 4(b)). While increasing the SBE results in a higher fraction of sputtered atoms escaping the body, this is counteracted by a corresponding decrease in the Na sputtering yield, resulting in a steep decline in the yield of escaped Na atoms for higher SBE values. The resulting escape yield using an Na SBE from albite is decreased by a factor of ∼12 and ∼9 for the Moon and Mercury, respectively, compared to the Na monoelemental E_{coh} and by a factor of ∼13 and ∼6 for the Moon and Mercury, respectively, compared to an Na SBE of 0.27 eV. Therefore, the exospheric composition of sputtered atoms depends both on the SBE of the sputtered atom and on the escape velocity of the celestial body being considered. As such, accurate SBE values are needed for reliably modeling the exospheric contribution of elements sputtered from the surface owing to SW impacts.

4. Summary

We have used MD theory to provide the first accurate SBE data we are aware of for Na sputtered for silicate minerals, which are expected to be important for exospheric formation at Mercury and the Moon. The MD SBE values for Na from the silicates albite and jadeite were ∼8 times larger than the Na monoelemental cohesive energy approximation. In addition, previously used models for SBEs from alloys were found to not be appropriate for mineral compounds. The increased SBE found from the MD calculations has a significant effect on the predicted SW ion sputtering yield and energy distribution of Na and the formation of the corresponding Na exosphere. As the SBE is increased, there is a decrease in the sputtering yield and an increase in the peak and width of the sputtered atom energy distribution. This shifted energy distribution affects the proportion of atoms sputtered with an energy above a planetary body's escape energy. Therefore, for collisional sputtering, the default SBE prescribed for multicomponent compounds by TRIM and SDTrimSP is not valid. Our mineral-specific SBEs will enable more accurate BCA predictions for the SW ion sputtering contribution to the Na exosphere of Mercury and the Moon.

We would like to thank G.E. Harlow for stimulating discussions. The material is based upon work supported by NASA under award number 80GSFC21M0002. R.M.K. and D.W.S. were supported, in part, by NASA Solar System Workings Program Award No. 80NSSC18K0521 and 80NSSC22K0099. R.M.K. and L.S.M. were partially supported by the NASA Solar System Exploration Research Virtual Institute team LEADER. O.J.T. was supported by the GSFC ISFM Exosphere Ionosphere Magnetosphere Modeling package.

Appendix
Comparing MD Results to Alloy Model

Our MD SBE results demonstrate that the cohesive energy SBE model of Gades & Urbassek (1994) for alloys cannot be applied to silicate minerals relevant to planetary science studies. Gades and Urbassek showed that the SBE scales linearly with elemental percentage in an alloy and is a function of the monoelemental cohesive energy of each element, varying as

$$U_A = c_A U_{AA} + c_B U_{AB}, \tag{A1}$$

where U_A is the SBE of element A in alloy AB, U_{AA} is the SBE of the pure element A, c_A and c_B are the concentrations of elements A and B, respectively, and U_{AB} is the SBE of a single surface impurity atom A in an otherwise-pure element B. U_{AB} can be expressed via

$$U_{AB} = \frac{Z_s}{Z}(E^A_{coh} + E^B_{coh}), \tag{A2}$$

where Z and Z_s are the coordination number for bulk and surface atoms, respectively, and E^A_{coh} and E^B_{coh} are the monoelemental cohesive energies of A and B, respectively, from Jain et al. (2013). This alloy model assumes that every element in the alloy can occupy any position in the lattice structure.

We have adapted the alloy model Equations (A1) and (A2) for minerals with three and four element types (A, B, C, D). In this case, the SBE of element type A in a compound A, B, C, D ($U_{A\text{-compound}}$) is expressed as

$$U_{A\text{-compound}} = c_A U_{AA} + c_B U_{AB} + c_C U_{AC} + c_D U_{AD}, \tag{A3}$$

where c_B, c_C, and c_D are the concentrations of elements B, C, and D, respectively, and U_{AX} is the SBE of a single surface impurity atom A in an otherwise-monoelemental solid X (either B, C, or D). U_{AX} can be expressed via

$$U_{AX} = \frac{Z_s}{Z}(E^A_{coh} + E^X_{coh}), \tag{A4}$$

where E^X_{coh} is the monoelemental cohesive energies of element X (either B, C, or D) from Jain et al. (2013). In alloys, $Z_s \leqslant Z$. Here we have calculated Z_s using the structures provided on the Materials Project database (Jain et al. 2013) and find that $Z_s = 3$ for Na in sodium orthosilicate, sodium metasilicate, and nepheline and that $Z_s = 4$ for Na in albite and jadeite. The corresponding values of Z are given in Table 1.

For high Na fractions, the alloy model and MD results are in fair agreement. But as can be seen in Figure A1, as the Na fraction decreases below 45% and the compound complexity increases, the alloy model of Gades & Urbassek underpredicts the Na SBE as compared to the MD results. We attribute these differences to the fact that each Na atom in the considered mineral compounds can only occupy a specific position in the

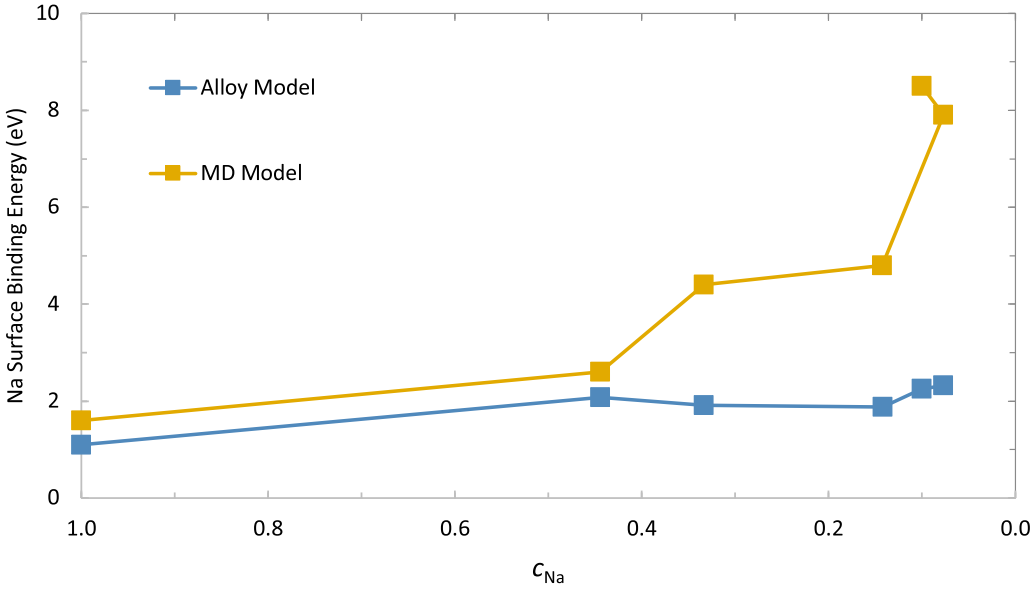

Figure A1. Na SBE as a function of the concentration of Na, c_{Na}, in the mineral using our MD results (yellow line) and the alloy model from Gades & Urbassek (1994; blue line). The lines are drawn to guide the eye.

lattice structure. Our findings demonstrate that the alloy model of Gades & Urbassek is not applicable to the silicate minerals that comprise the surfaces of rocky planetary bodies.

ORCID iDs

Liam S. Morrissey https://orcid.org/0000-0001-7860-9957
Orenthal J. Tucker https://orcid.org/0000-0002-8235-5440
Rosemary M. Killen https://orcid.org/0000-0002-0543-2326
Sam Nakhla https://orcid.org/0000-0001-8388-454X
Daniel W. Savin https://orcid.org/0000-0002-1111-6610

References

Assmann, W., Toulemonde, M., & Trautmann, C. 2007, in Sputtering by Particle Bombardment, ed. R. Behrisch & W. Eckstein (Berlin: Springer), 401
Behrisch, R., & Eckstein, W. 2007, Sputtering by Particle Bombardment: Experiments and Computer Calculations from Threshold to MeV Energies, 110 (Berlin: Springer)
Berendsen, H. J. C., Postma, J. P. M., van Gunsteren, W. F., DiNola, A., & Haak, J. R. 1984, JChPh, 81, 3684
Betz, G. 1987, NIMPB, 27, 104
Bringuier, S., Abrams, T., Guterl, J., et al. 2019, Nucl. Mater. Energy, 19, 1
Burger, M. H., Killen, R. M., Vervack, R. J., Jr., et al. 2010, Icar, 209, 63
Cassidy, T. A., McClintock, W. E., Killen, R. M., et al. 2016, GeoRL, 43, 11
Colaprete, A., Sarantos, M., Wooden, D. H., et al. 2016, Sci, 351, 249
Darden, T., York, D., & Pedersen, L. 1993, JChPh, 98, 10089
Domingue, D. L., Chapman, C. R., Killen, R. M., et al. 2014, SSRv, 181, 121
Dukes, C. A., & Baragiola, R. A. 2015, Icar, 255, 51
Dukes, C. A., Chang, W.-Y., Famá, M., & Baragiola, R. A. 2011, Icar, 212, 463
Eckstein, W. 2007, in Sputtering by Particle Bombardment, ed. R. Behrisch & W. Eckstein (Berlin: Springer), 33
Eckstein, W., & Urbassek, H. M. 2007, in Sputtering by Particle Bombardment, ed. R. Behrisch & W. Eckstein (Berlin: Springer), 21
Elphic, R. C., Funsten, H. O., III, Barraclough, B. L., et al. 1991, GeoRL, 18, 2165
Fatemi, S., Poppe, A. R., & Barabash, S. 2020, JGRA, 125, e2019JA027706
Gades, H., & Urbassek, H. M. 1994, NIMPB, 88, 218
Gamborino, D., Vorburger, A., & Wurz, P. 2019, AnGeo, 37, 455
Grischkowsky, D., Ming, L. Y., & Balant, A. C. 1983, SurSc, 127, 315
Gschneidner, K. A., Jr. 1964, Solid State Phys., 16, 275
Hahn, S. H., Rimsza, J., Criscenti, L., et al. 2018, J. Phys. Chem. C, 122, 19613
Jackson, D. P. 1973, Radiat. Eff., 18, 185
Jackson, D. P. 1975, CaJPh, 53, 1513
Jain, A., Ong, S. P., Hautier, G., et al. 2013, APLM, 1, 11002
Johnson, R. E. 2013, Energetic Charged-particle Interactions with Atmospheres and Surfaces, 19 (Berlin: Springer)
Kallio, E., Dyadechkin, S., Wurz, P., & Khodachenko, M. 2019, P&SS, 166, 9
Kelly, R. 1986, NIMPB, 18, 388
Killen, R., Cremonese, G., Lammer, H., et al. 2007, SSRv, 132, 433
Killen, R. M., & Ip, W. 1999, RvGeo, 37, 361
Killen, R. M., Morgan, T. H., Potter, A. E., et al. 2019, Icar, 328, 152
Killen, R. M., Morgan, T. H., Potter, A. E., et al. 2021, Icar, 355, 114155
Killen, R. M., Potter, A. E., Reiff, P., et al. 2001, JGRE, 106, 20509
Killen, R. M., Sarantos, M., Potter, A. E., & Reiff, P. 2004, Icar, 171, 1
Kittel, C., McEuen, P., & McEuen, P. 1996, Introduction to Solid State Physics, 8 (New York: Wiley)
Krasheninnikov, A. V., & Nordlund, K. 2010, JAP, 107, 3
Lammer, H., Wurz, P., Patel, M. R., et al. 2003, Icar, 166, 238
Leblanc, F., Doressoundiram, A., Schneider, N., et al. 2008, GeoRL, 35, L18204
Leblanc, F., & Johnson, R. E. 2003, Icar, 164, 261
Lundquist, T. R. 1978, JVST, 15, 684
Lyngdoh, G. A., Kumar, R., Krishnan, N. M. A., & Das, S. 2019, JChPh, 151, 64307
Madey, T. E., Yakshinskiy, B. V., Ageev, V. N., & Johnson, R. E. 1998, JGRE, 103, 5873
Martinez, R., Langlinay, T., Ponciano, C. R., et al. 2017, NIMPB, 406, 523
Mazarov, P., Samartsev, A. V., & Wucher, A. 2006, ApSS, 252, 6452
McClintock, W. E., Cassidy, T. A., Merkel, A. W., et al. 2018, Mercur View after MESSENGER (Cambridge: Cambridge Univ. Press), 371
McCoy, T. J., Peplowski, P. N., McCubbin, F. M., & Weider, S. Z. 2018, Mercur View after MESSENGER (Cambridge: Cambridge Univ. Press), 176
McGrath, M. A., Johnson, R. E., & Lanzerotti, L. J. 1986, Natur, 323, 694
Mineral Data Publishing 2001, RRUFF, Albite, (USA:Mineral Data Publishing 2001), (https://rruff.info/doclib/hom/albite.pdf)
Möller, W., & Posselt, M. 2001, TRIDYN_FZR User Manual (Dresden: FZR)
Morrissey, L. S., Tucker, O. J., Killen, R. M., Nakhla, S., & Savin, D. W. 2021, JAP, 130, 13302
Mortier, W. J., Ghosh, S. K., & Shankar, S. 1986, JChPh, 108, 4315
Mouawad, N., Burger, M. H., Killen, R. M., et al. 2011, Icar, 211, 21
Mura, A., Milillo, A., Orsini, S., & Massetti, S. 2007, P&SS, 55, 1569
Mura, A., Wurz, P., Lichtenegger, H. I. M., et al. 2009, Icar, 200, 1
Mutzke, A., Schneider, R., Eckstein, W., et al. 2019, SDTrimSP Version 6.00. doi:10.17617/2.3026474
Papike, J., Taylor, L., & Simon, S. 1991, Lunar Sourcebook, A User's Guide to Moon (Cambridge: Cambridge Univ. Press), 121
Peplowski, P. N., Evans, L. G., Stockstill-Cahill, K. R., et al. 2014, Icar, 228, 86

Pieters, C. M., Edwards, J. O., Clay, C., et al. 2009, Sci, 326, 568
Pitman, M. C., & Van Duin, A. C. T. 2012, JaChS, 134, 3042
Plimpton, S. J. 1995, JCoPh, 117, 1
Poppe, A. R., Farrell, W. M., & Halekas, J. S. 2018, JGRE, 123, 37
Potter, A. E., & Morgan, T. H. 1988, Sci, 241, 675
Raines, J. M., Gershman, D. J., Zurbuchen, T. H., et al. 2013, JGRA, 118, 1604
Sarantos, M., Killen, R. M., & Kim, D. 2007, P&SS, 55, 1584
Schaible, M. J., Dukes, C. A., Hutcherson, A. C., et al. 2017, JGRE, 122, 1968
Schmidt, C. A., Baumgardner, J., Mendillo, M., & Wilson, J. K. 2012, JGRA, 117, A03301
Schmidt, C. A., Baumgardner, J., Moore, L., et al. 2020, PSJ, 1, 4
Song, H. Y., Zhang, L., & Xiao, M. X. 2016, PhLA, 380, 4049
Sprague, A. L., Emery, J. P., Donaldson, K. L., et al. 2002, M&PS, 37, 1255
Szabo, P. S., Biber, H., Jäggi, N., et al. 2020, ApJ, 891, 100
Tenishev, V., Rubin, M., Tucker, O. J., Combi, M. R., & Sarantos, M. 2013, Icar, 226, 1538
Thompson, M. W. 1968, PMag, 18, 377
Tucker, O. J., Farrell, W. M., & Poppe, A. R. 2021, JGRE, 126, e2020JE006552
Urbassek, H. M. 2007, in Sputtering by Particle Bombardment, ed. R. Behrisch & W. Eckstein (Berlin: Springer), 189
Van Duin, A. C. T., Dasgupta, S., Lorant, F., & Goddard, W. A. 2001, JPCA, 105, 9396
Vervack, R. J., McClintock, W. E., Killen, R. M., et al. 2010, Sci, 329, 672
Werner, A. L. E., Aizawa, S., Leblanc, F., et al. 2022, Icar, 372, 114734
Wiens, R. C., Burnett, D. S., Calaway, W. F., et al. 1997, Icar, 128, 386
Wolf, D., Keblinski, P., Phillpot, S. R., & Eggebrecht, J. 1999, JChPh, 110, 8254
Wurz, P., Whitby, J. A., Rohner, U., et al. 2010, P&SS, 58, 1599
Yamamura, Y., & Tawara, H. 1996, ADNDT, 62, 149
Yang, X., & Hassanein, A. 2014, ApSS, 293, 187
Ziegler, J. F., & Biersack, J. P. 1985, in Treatise on Heavy-ion Science, ed. D. A. Bromley (Berlin: Springer), 93